metals

MDPI

Article

Effect of Cryogenic Treatment on Microstructure and Mechanical Properties of $Al_{0.6}CrFe_2Ni_2$ Dual-Phase High-Entropy Alloy

Sichen Xie [1,2], Qingyao Lv [1,2], Wei Zhang [1,2,*], Yingdong Qu [1,2,*], Hao Qi [1,2], Bo Yu [3], Rongde Li [1,2], Guanglong Li [1,2] and Fei Yang [4]

1 School of Materials Science and Engineering, Shenyang University of Technology, Shenyang 110870, China
2 State Key Laboratory of Light Metals of Liaoning, Shenyang University of Technology, Shenyang 110870, China
3 State Key Laboratory of Light Alloy Casting Technology for High-End Equipment, Shenyang 110022, China
4 Waikato Centre for Advanced Materials and Manufacturing, School of Engineering, University of Waikato, Hamilton 3240, New Zealand
* Correspondence: author: zwei@sut.edu.cn (W.Z.); quydong@sut.edu.cn (Y.Q.)

Abstract: The contradiction between strength and ductility limits the application of high-entropy alloys (HEAs). To simultaneously improve the strength and ductility of HEAs, the cryogenic treatment was proposed and applied in this paper. The $Al_{0.6}CrFe_2Ni_2$ HEA with dual-phase structure was selected as the experimental material for cryogenic treatment. The microstructure and mechanical properties of the HEA in an as-cast and cryogenically treated state were analyzed in detail. The results showed that the grain size of equiaxed crystal in the alloy decreased continuously by prolonging the cryogenic treatment time, and the average value was 44.6 μm for the cryogenically treated HEA at the time of 48 h, which was 46.5% lower than that of the as-cast alloy. The number and size of ordered body-centered cubic (B2) spherical nanophases embedded in the body-centered cubic (BCC) structured inter-dendritic region, however, increased continuously by extending the cryogenic treatment time. The cryogenic treatment also made more slip systems activate, cross-slip occurred in the alloy, and a large number of stacking faults were found in the transmission electron microscopy (TEM) microstructure for the alloy that underwent a long time in cryogenic treatment. The yield strength of the $Al_{0.6}CrFe_2Ni_2$ HEA was gradually increased with the increase in cryogenic treatment time, and the maximum yield strength of the 48 h cryogenically treated alloy was 390 MPa, which was 39.3% higher than that of the as-cast. This increase in mechanical properties after cryogenic treatment was attributed to the refinement of grains and the large precipitation of nanophases, as well as the appearance of cross-slips and stacking faults caused by cryogenic treatment.

Keywords: high-entropy alloys; cryogenic treatment; mechanical properties; nanophases

check for updates

Citation: Xie, S.; Lv, Q.; Zhang, W.; Qu, Y.; Qi, H.; Yu, B.; Li, R.; Li, G.; Yang, F. Effect of Cryogenic Treatment on Microstructure and Mechanical Properties of $Al_{0.6}CrFe_2Ni_2$ Dual-Phase High-Entropy Alloy. *Metals* **2023**, *13*, 195. https://doi.org/10.3390/met13020195

Academic Editor: Andrea Di Schino

Received: 7 December 2022
Revised: 9 January 2023
Accepted: 11 January 2023
Published: 18 January 2023

Copyright: © 2023 by the authors. Licensee MDPI, Basel, Switzerland. This article is an open access article distributed under the terms and conditions of the Creative Commons Attribution (CC BY) license (https://creativecommons.org/licenses/by/4.0/).

1. Introduction

Since the concept of high-entropy alloys (HEAs) was proposed, HEAs have rapidly become a research hotspot due to their excellent properties such as high strength and ductility [1–5], high friction and wear resistance [6,7], and good corrosion resistance [8,9]. To improve the strength and ductility of HEAs simultaneously, scholars have conducted detailed studies on composition design [10], the addition of ceramic phases [11], laser additive [12], rolling [13], and heat treatment [14]. Shen et al. [15] studied the evolution of microstructure and mechanical properties of non-equimolar dual-phase Al-Co-Cr-Fe-Ni HEA after heat treatment. The results indicated that the appropriate heat treatment temperature could promote the increase in precipitated phase in the solid solution, thereby improving the hardness and yield strength of the alloy. Mehranpour et al. [16] investigated

the microstructure evolution of single-phase CoCrFeNiMn HEAs during short-term post-deformation annealing (PDA), and the results showed that the strength of the material was significantly improved due to the formation of precipitates at a suitable heat treatment temperature. Malatji et al. [17] investigated the effect of heat treatment temperature on the microstructure, microhardness, and wear properties of the AlCrFeCuNi HEAs. The results showed that the heat treatment at the temperatures ranging from 800 °C to 1100 °C could improve the homogenization of the phase. Although the specimens had uniform microhardness and friction properties after treatment at an appropriate temperature, their ductility was relatively low. Munitz et al. [18] explored the microstructure and mechanical properties of $AlCrFeNiTi_{0.5}$ at different heat treatment temperatures. The results showed that several phase transformations and morphological changes occurred in the alloy during heat treatment at an appropriate temperature, and the strength and plasticity of the alloy were improved. It can be seen that heat treatment can effectively ameliorate the strength or ductility of HEAs. Namely, the strength or ductility of HEAs can be modulated by changing the treatment temperature; however, it is difficult to achieve the simultaneous enhancement of strength and ductility.

The cryogenic treatment technology, as one type of heat treatment, is widely used in traditional alloys to improve both the strength and ductility by refining grains and homogenizing microstructures. Li et al. [19] researched the effect of cryogenic treatment on the microstructure and mechanical properties of a low-carbon high-alloy martenitic bearing steel. The results indicated that the cryogenic treatment not only accelerated the transformation of retained austenite to martensite, but also promoted the formation of fine carbide particles, resulting in a higher hardness of the specimen than that of the traditional heat treatment specimen. Wannaprawat et al. [20] studied the impact of cryogenic treatment holding time on the transformation of CuNi precipitates and CuNiZr precipitates of the CuBeZr alloy. The study found that prolonging the immersion time of samples in liquid nitrogen would promote the shape of the precipitates from spherical to rod-like and increase the number of precipitates distributed around the α-phase matrix. This change in microstructure resulted in an increase in hardness and preferable wear resistance. Cardoso et al. [21] explored the effect of cryogenic treatment on the microstructure, impact toughness and wear resistance of AISI D6 tool steel. The results showed that cryogenic treatment and secondary tempering could reduce the content of residual austenite, increase the content of carbide, and make a more uniform distribution, thereby promoting the simultaneous improvement of strength and hardness. The above studies show that the cryogenic treatment technology can not only improve the uniformity of the microstructure and chemical composition of traditional alloys but also achieve the simultaneous improvement of their mechanical properties.

The research on the effect of cryogenic treatment on HEAs, however, is rarely reported even though its application in traditional materials has been relatively mature. Li et al. [22] studied the effect of cryogenic treatment on the microstructure and mechanical properties of $AlCrFe_2Ni_2$ HEA. The results showed that the grain orientation of BCC and B2 phases in the alloy changed and transformed into each other by increasing the cryogenic treatment time. The banded FCC phase structure became shorter and more disordered, and the strength and ductility of the alloy were improved simultaneously. However, the reasons for the changes in the mechanical properties and microstructure of the HEA caused by cryogenic treatment have not been analyzed in detail.

In this paper, using the dual-phase structured $Al_{0.6}CrFe_2Ni_2$ HEA ingots prepared by arc melting as the experimental material, a series of cryogenic treatments with different cryogenic treatment time were carried out, and the effect of cryogenic treatment on the microstructure and mechanical properties of the HEA is studied in detail. The reasons for improving the properties of HEA are analyzed from the perspective of microstructure and dislocation changes caused by cryogenic treatment. This work may provide a significant theoretical basis and practical experience for improving both the strength and the ductility of HEAs.

2. Experimental Materials and Methods

Al, Cr, Fe and Ni with a purity of 99.99% were used as raw materials, and a non-consumable electric arc melting furnace (ZKVAF-1250) was used to prepare the $Al_{0.6}CrFe_2Ni_2$ (at.%) ingot. The raw materials were weighed (about 100 g for each ingot) according to the nominal composition, and then, they were placed into a hemispherical water-cooled copper crucible with a diameter of 50 mm in the order of lowest-melting-point material to highest-melting-point material. The vacuum system of the vacuum arc furnace was firstly used to ensure the furnace environment reached a vacuum level of 5×10^{-3} Pa, and then, pure argon was filled into the furnace before the materials were heated until the vacuum degree reached 50 kPa. All ingots were melted repeatedly at least five times at the current intensity of 450 A to ensure the uniformity of chemical composition distribution throughout the ingot, and the basic same microstructure of all ingots. A selection of the HEA ingots cooled to room temperature were then placed into liquid nitrogen (−196 °C) for cryogenic treatment, and the cryogenic treatment time was set to 4 h, 8 h, 12 h, 24 h, and 48 h, respectively, after which, the ingots were quickly removed from the liquid nitrogen and returned to room temperature in the air. Three groups of ingots were used to undergo each cryogenic treatment condition to ensure the repeatability of the research.

Specimens in the shape of cubes ($10 \times 10 \times 10$ mm) and cylinders (Ø4×6 mm) were cut from the as-cast and cryogenically treated ingots, which were used for microstructure observation and mechanical properties testing, respectively. Prior to microstructure observation, the specimens were subjected to mechanical polishing and electrolytic polishing. The electrolytic solution was prepared by mixing 10% perchloric acid and 90% glacial acetic acid. The phase and crystal structure of the alloys were identified via X-ray diffractometry (XRD) using a Shimadzu 7000 diffractometer (Kyoto, Japan) with the scan rate of 4°/min from 20° to 100°. The microstructure of the alloys in as-cast and cryogenically treated state was observed with a 3D measurement laser microscope (LEXT OLS4100) and transmission electron microscopy (TEM, JEM-2100). The grain size was measured from the microstructure diagram using the CorelDRAW software and the Image-Pro Plus software. The CorelDRAW software was firstly used to outline the contour of a single grain in the microstructure diagram, and then, the Image-Pro Plus software was used to measure the grain size through the core of the grain at a 2-degree interval. The room temperature compression tests were conducted on the universal electronic testing machine (MTS-E45) with a strain rate of 1×10^{-3} s^{-1}. The compression experiments of the samples in each state were tested five times to ensure repeatability.

3. Results and Discussion

3.1. The Dependence of Phase Composition on Cryogenic Treatment

Figure 1 shows the XRD diffraction patterns of the $Al_{0.6}CrFe_2Ni_2$ HEA in the as-cast state and the cryogenically treated state treated at different cryogenic treatment times. It can be seen that the as-cast and cryogenically treated $Al_{0.6}CrFe_2Ni_2$ HEAs are composed of the face-centered cubic (FCC) structure phase, body-centered cubic (BCC) structure phase, and ordered body-centered cubic (B2) structure phase, indicating that cryogenic treatment does not change the phase composition of the alloy. The diffraction peaks at 2θ values of 43.5°, 50.7°, 74.5°, and 90.5° are indexed as (111), (200), (220), and (311) crystal planes, respectively, which correspond to the FCC phase. The peaks at the 2θ value of 44.6° are indexed to be the (110) crystal plane and correspond to the BCC phase and B2 phase. The similar crystal structure and lattice constant of the BCC phase and B2 phase leads to the overlap of diffraction peaks. This phase composition of the $Al_{0.6}CrFe_2Ni_2$ HEA in different states measured via XRD is similar to that of the AlCrFe2Ni2 reported in Ref. [22], indicating that the microstructure of this series of alloys has a certain similarity.

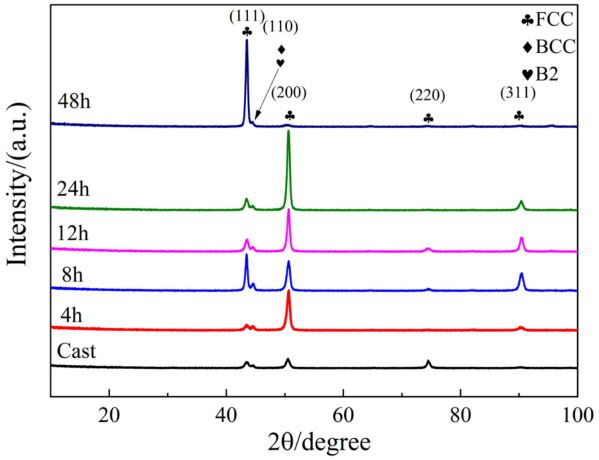


Figure 1. XRD patterns of $Al_{0.6}CrFe_2Ni_2$ HEAs at as-cast and cryogenically treated states.

It is worth noting that although the cryogenic treatment does not change the composition of the crystal structure in the alloy, the diffraction peak intensity of each crystal structure and its corresponding crystal plane changes significantly. The most conspicuous changes in diffraction peak intensity are the (111) and (200) crystal planes. Compared with the as-cast $Al_{0.6}CrFe_2Ni_2$ HEA, the diffraction peak intensity of the (111) crystal plane decreases slightly for the alloy cryogenically treated at the time of 4 h, increases significantly for the alloy treated at 8 h, and slightly increases for both the alloys treated at 12 h and 24 h. The HEA cryogenically treated for 48 h has the highest intensity of the (111) peak among all the investigated alloys. The diffraction peak intensity of the (200) crystal plane gradually increases with increasing the time of cryogenic treatment from 4 h to 24 h. However, the (200) peak intensity is significantly low for the 48 h treated alloy, even lower than the as-cast alloy. This phenomenon of diffraction peak intensity change often occurs in the cryogenic treatment of magnesium alloys and other alloys, and it is considered to be the result of grain rotation, which is mainly related to the internal stress caused by the volume shrinkage during cryogenic treatment [23,24]. The grain rotation caused by cryogenic treatment makes it impossible to analyze the change trend of the proportion or size of the three groups of phases in the alloy through the change rule of intensity or half-height width of the diffraction peaks in the XRD patterns. Therefore, the intuitive microstructure observation needs further exploration in this work.

3.2. Effect of Cryogenic Treatment on Microstructure

Figure 2 shows the microstructures of as-cast and cryogenically treated $Al_{0.6}CrFe_2Ni_2$ HEAs observed by the 3D measurement laser microscope. It can be seen that both the as-cast and cryogenically treated $Al_{0.6}CrFe_2Ni_2$ HEAs are composed of equiaxed crystal matrix structure and intergranular structure on a relatively macroscopic scale. Combined with the XRD pattern, it is not difficult to speculate that the equiaxed crystal matrix structure with a large volume ratio should correspond to the FCC phase with the highest diffraction peak intensity as shown in Figure 1, and the intergranular structure with a small volume ratio should be mainly composed of BCC and/or B2 phases. In addition, it can be seen from Figure 2 that the size of the equiaxed crystal structure is significantly affected by the cryogenic treatment time. The average equiaxed grain size of the as-cast alloy measured from Figure 2a using the CorelDRAW software and the Image-Pro Plus software is 83.3 μm. After cryogenic treatment, the equiaxed grain size decreases, and the longer the cryogenic treatment time, the smaller the equiaxed grain size. When the cryogenic treatment time reaches 48 h, the equiaxed grain size decreases to 44.6 μm, which is 46.5% lower than that of the as-cast alloy. This grain refinement caused by cryogenic treatment is related to the plastic deformation of the microstructure, promoted by the cooling internal stress in the crystal during cryogenic treatment [25], as well as the superposition of the strong lattice

distortion of the alloy. Note that although the three-dimensional confocal microstructure can analyze the crystal distribution in the alloy, it is difficult to observe the structure of the alloy at a more microscopic scale. For example, do the BCC phase and B2 phase with overlapping diffraction peaks in the XRD patterns exist simultaneously? How are they distributed? Such microstructure needs further exploration.

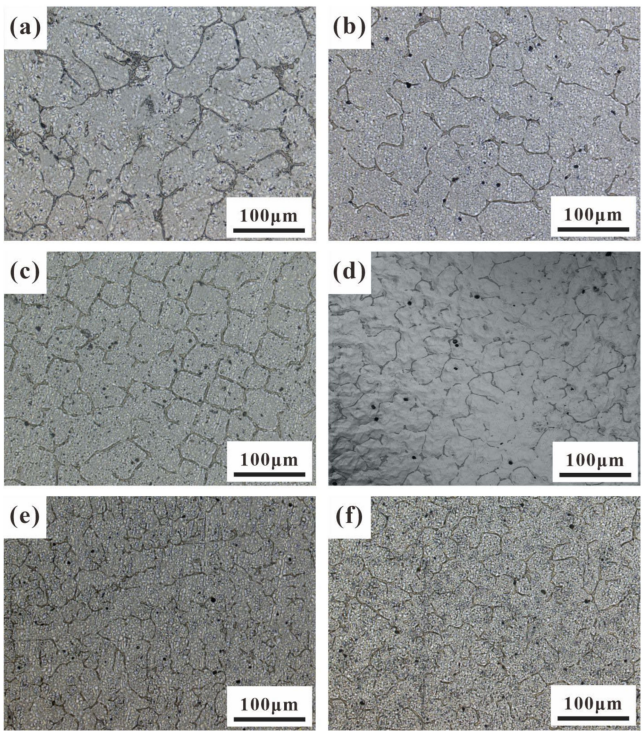


Figure 2. Three-dimensional confocal microstructure of $Al_{0.6}CrFe_2Ni_2$ HEAs in as-cast and cryogenically treated states: (**a**) as-cast; (**b**) cryogenic treatment for 4 h; (**c**) cryogenic treatment for 8 h; (**d**) cryogenic treatment for 12 h; (**e**) cryogenic treatment for 24 h; (**f**) cryogenic treatment for 48 h.

Figure 3 shows the TEM morphology and the corresponding electron diffraction patterns of the $Al_{0.6}CrFe_2Ni_2$ HEAs in the as-cast state and cryogenically treated state (t_{treat} = 48 h). The regions A and C in Figure 3a are the morphology of inter-dendrite and dendrite in the $Al_{0.6}CrFe_2Ni_2$ HEA, respectively. A large number of nano-scale black particle phases are observed in the inter-dendritic structure, which are set as regions B, and they do not exist in the dendritic structure. The electron diffraction analysis reveals that the inter-dendrite (region A) and the nano-scale black particle phases (region B) are disordered body-centered cubic crystal structures and ordered body-centered cubic crystal structures, which are denoted as BCC and B2, respectively. The crystal structure of region C is determined to be FCC structure. The selected areas of electron diffraction results are consistent with the crystal structure results obtained via XRD analysis, i.e., the $Al_{0.6}CrFe_2Ni_2$ HEA is composed of BCC, B2, and FCC phases. The phase composition of the alloy after cryogenic treatment for 48 h is not significantly different from that of the as-cast alloy, as shown in Figure 3b, and the result is consistent with the XRD analysis as well. The TEM morphology and selected area electron diffraction results of the as-cast and cryogenically treated HEAs confirm that the cryogenic treatment does not change the phase composition of the alloy. At the same time, it indicates that the equiaxed grains in the three-dimensional confocal structure of the alloy at a relatively macroscopic scale are FCC phases, and the intergranular structure between the equiaxed grains is composed of BCC phases and a large number of B2 phases embedded in the BCC phases.

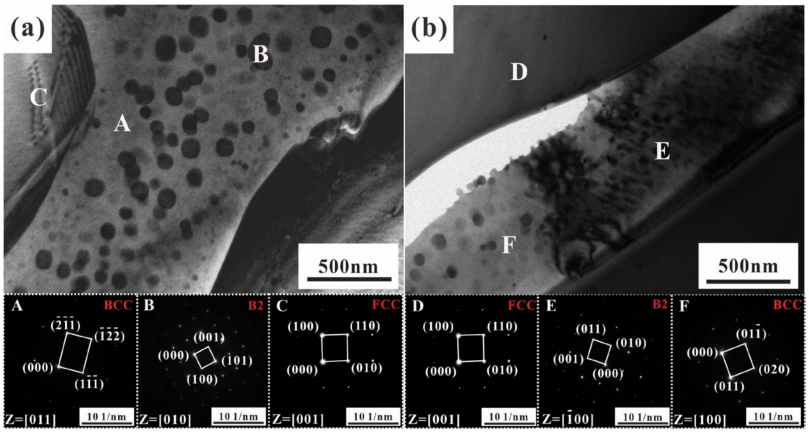


Figure 3. TEM images and electron diffraction patterns of $Al_{0.6}CrFe_2Ni_2$ HEAs in as-cast and cryogenically treated states: (**a**) as-cast; (**b**) cryogenic treatment for 48 h. The electron diffraction patterns correspond to the regions in the TEM images. Region A and F correspond to the inter-dendritic BCC structure; region B and E correspond to the spherical B2 nanophases embedded in the inter-dendritic structure; region C and D correspond to the FCC crystal structure.

Figure 4 shows the bright-field TEM images of the inter-dendritic regions of the as-cast and cryogenically treated $Al_{0.6}CrFe_2Ni_2$ HEAs. A large number of black spherical nanophases (B2) are distributed at the inter-dendritic regions of all alloys. The average size and number density of these B2 nanophases are gradually increased with the increase in cryogenic treatment time. The average size of the B2 nanophases in the as-cast alloy measured through the core of the grain at a 2-degree interval by using the Image-Pro Plus software is about 95.6 nm, and the value for the 48 h treated alloy is about 148.2 nm, which is 55% higher than that of the as-cast alloy. In addition, the 48 h treated alloy has the greatest number density of B2 nanophases compared with the other alloys, covering almost the whole inter-dendritic region. The change in the number and size of B2 phases in the inter-dendritic region of $Al_{0.6}CrFe_2Ni_2$ HEA is attributed to the plastic deformation within the grain caused by the volume shrinkage during cryogenic treatment. Part of the deformation energy is converted into internal energy, which strengthens the driving force for the precipitation of nanophases.

During cryogenic treatment, the alloy undergoes volume shrinkage and certain plastic deformation, which in turn causes microscopic changes in dislocation morphology in the alloy. These microscopic changes and interactions in the dislocation provide more nucleation sites for the precipitation of nanophases [26]. Figure 5 shows the dislocation morphologies of the as-cast and cryogenically treated $Al_{0.6}CrFe_2Ni_2$ HEAs. It can be seen that a small number of dislocations are dispersed in the as-cast alloy (Figure 5a), which are caused by the rapid solidification and cooling of the alloy melt by the water-cooled copper crucible during ingot preparation. For the HEAs in cryogenic treatment for 4 and 8 h, the dislocation density and length increase significantly, and obvious dislocation tangles and accumulations are observed at the grain boundaries (Figure 5b,c). This is caused by the increase in the alloy's plastic deformation induced by the cryogenic treatment. With increasing the cryogenic treatment to 12 and 24 h, a large number of dislocations move along the same slip plane to form slip bands in the alloys under larger cryogenic treatment-induced plastic deformation, compared to the alloys in cryogenic treatment for 4 and 8 h. As shown in Figure 5e, two sets of slip bands are found. This indicates that the large degree of plastic deformation of the alloy causes the crystal surface to rotate, resulting in dislocation slip occurring on two or more sliding surfaces at the same time. With further increasing in the cryogenic treatment time to 48 h, we can speculate that significant plastic deformation happens in the alloy due to a longer period of cryogenic treatment, which will result in more slip systems being activated and cross-slips occurring, as confirmed by the large number of stacking faults observed in Figure 5f.

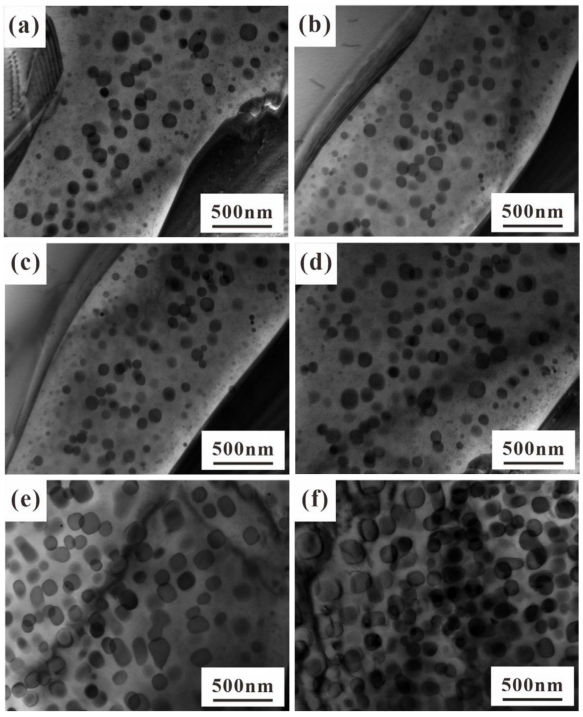


Figure 4. Bright-field TEM image of inter-dendritic regions of $Al_{0.6}CrFe_2Ni_2$ HEAs in different states: (**a**) as-cast; (**b**) cryogenic treatment for 4 h; (**c**) cryogenic treatment for 8 h; (**d**) cryogenic treatment for 12 h; (**e**) cryogenic treatment for 24 h; (**f**) cryogenic treatment for 48 h.

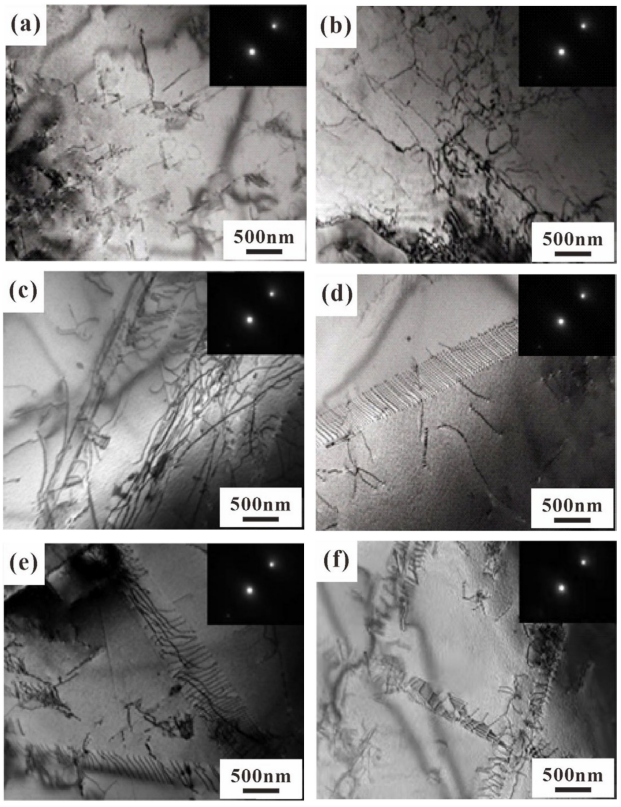


Figure 5. TEM images of dislocation morphology in as-cast and cryogenically treated $Al_{0.6}CrFe_2Ni_2$ HEAs: (**a**) as-cast; (**b**) cryogenic treatment for 4 h; (**c**) cryogenic treatment for 8 h; (**d**) cryogenic treatment for 12 h; (**e**) cryogenic treatment for 24 h; (**f**) cryogenic treatment for 48 h.

3.3. Effect of Cryogenic Treatment on Compression Performance

The above microstructure analysis shows that the grain size, the number density and size of B2 phase, and the dislocation morphology in the matrix structure of the $Al_{0.6}CrFe_2Ni_2$ HEA strongly depend on the cryogenic treatment time, which indicates that the mechanical properties of the alloy will also change with the cryogenic treatment conditions. Figure 6a shows the compression curves of the as-cast and the cryogenically treated $Al_{0.6}CrFe_2Ni_2$ HEAs. It can be seen that the $Al_{0.6}CrFe_2Ni_2$ HEAs in all states exhibit excellent ductility, and no fracture occurs even when the compressive strain reaches 45%. This is because the generation and movement of dislocations and stacking faults in the HEAs during compressive plastic deformation always change with the stress fluctuation, in which the occurrence of cross-slips and stacking faults makes the HEAs have better strength and ductility [27]. Figure 6b shows the enlarged compressive curves at a strain ranging from 0 to 10%, which makes the change law of the HEAs in the compression yield stage clearer and more intuitive. The inset in Figure 6b shows the dependence of yield strength on the cryogenic treatment time, and it can be observed that the yield strength of the alloy is increased with the increase in cryogenic treatment time. When the cryogenic treatment time is 48 h, the maximum yield strength of the alloy is 390 MPa, which is 39.3% higher than that of the as-cast (280 MPa).

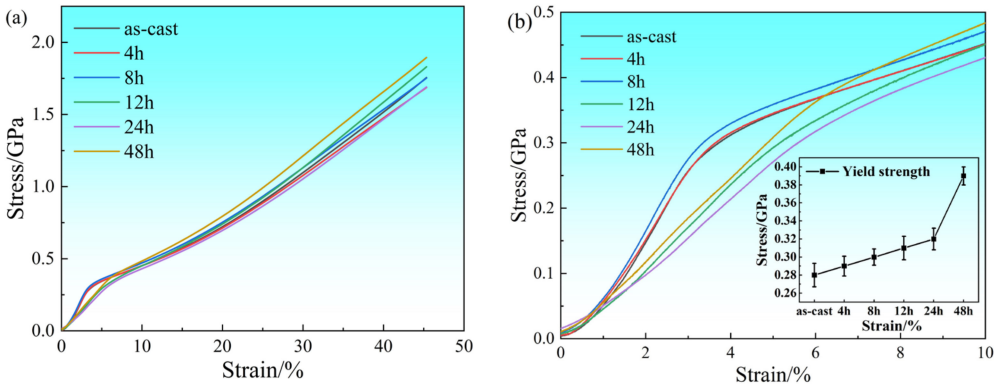


Figure 6. The compressive stress–strain curves of as-cast and cryogenically treated $Al_{0.6}CrFe_2Ni_2$ HEAs: (**a**) the stress–strain curves with a strain range from 0 to 45%; (**b**) the enlarged stress–strain curves at yield stage. The inset in Figure (**b**) shows the dependence of yield strength on the cryogenic treatment time.

Combined with the evolution of microstructure and dislocation shown in Figure 7, the mechanism of cryogenic treatment improving the mechanical properties of the $Al_{0.6}CrFe_2Ni_2$ HEA can be described as follows. The schematic diagram mainly explains the strengthening mechanism from three aspects: grain refinement, B2 nanophase precipitation strengthening, and dislocation strengthening. For as-cast $Al_{0.6}CrFe_2Ni_2$ HEA, the grains are relatively coarse, and the number density of the B2 phase and dislocation is relatively small. With the advancement of cryogenic treatment and the extension of cryogenic treatment time, the cooling internal stress is generated inside the crystal of the alloy, which promotes the plastic deformation of the structure and refines the grains. In addition, the number and size of spherical B2 nanophases are increased. From the perspective of dislocation, the plastic deformation caused by short-term (4 h and 8 h) cryogenic treatment will aggravate the increase of dislocation density in the alloy, while a longer cryogenic treatment time will lead to the activation of a large number of slip systems (for alloys treated at the time more than 12 h) or even the appearance of cross-slips and stacking faults. In short, the increase in mechanical properties after cryogenic treatment is attributed to the refinement of grains and the precipitation of nanophases, as well as the appearance of cross-slips and stacking faults caused by cryogenic treatment.

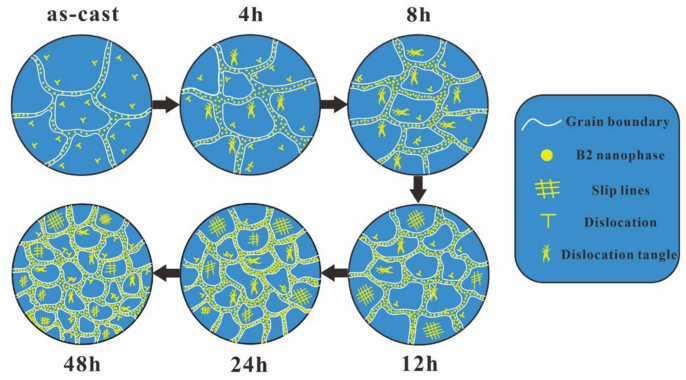


Figure 7. Microstructure evolution and strengthening mechanism of $Al_{0.6}CrFe_2Ni_2$ HEA caused by cryogenic treatment.

4. Conclusions

In this paper, the $Al_{0.6}CrFe_2Ni_2$ dual-phase high entropy alloy ingots were prepared using arc melting furnace under argon atmosphere, and then they were performed with cryogenic treatment at the time of 4 h, 8 h, 12 h, 24 h, and 48 h, respectively. The microstructure evolution and mechanical properties of the HEA strengthened by cryogenic treatment at different times were systemically studied, and the following conclusions are drawn:

(1) Cryogenic treatment can significantly refine the equiaxed grain size of the $Al_{0.6}CrFe_2Ni_2$ HEA, and the longer the cryogenic treatment time, the smaller the equiaxed grain size. When the cryogenic treatment time is 48 h, the average size of equiaxed grains decreases to 44.6 μm, which is 46.5% lower than that of the as-cast alloy.

(2) The $Al_{0.6}CrFe_2Ni_2$ HEA is composed of FCC phases, BCC inter-dendritic phases, and spherical B2 nanophases embedded in the BCC inter-dendritic region. The number and size of the B2 nanophases increase significantly with the increase in the cryogenic treatment time, which is related to the significant increase in dislocation density caused by volume shrinkage and plastic deformation of the alloy during cryogenic treatment.

(3) The refinement of equiaxed grains, the large precipitation of nanophases, and the appearance of cross-slips and stacking faults caused by cryogenic treatment give the $Al_{0.6}CrFe_2Ni_2$ HEA excellent strength and ductility. The 48 h cryogenically treated alloy shows a yield strength of 390 MPa, which is 39.3% higher than that of the as-cast alloy.

Author Contributions: Conceptualization, Y.Q.; methodology, W.Z.; software, S.X. and Q.L.; validation, G.L., B.Y. and F.Y.; formal analysis, H.Q.; investigation, S.X. and Q.L.; resources, R.L.; data curation, S.X.; writing—original draft preparation, S.X.; writing—review and editing, W.Z. and F.Y.; visualization, H.Q.; supervision, G.L.; project administration, Y.Q.; funding acquisition, Y.Q. All authors have read and agreed to the published version of the manuscript.

Funding: This work was funded by the Open Project of State Key Laboratory of Light Alloy Casting Technology for High-end Equipment [LACT-009] and the Natural Science Foundation of Liaoning Province [2020-KF-14-03].

Data Availability Statement: The date presented in this study are available within the article.

Conflicts of Interest: The authors declare no conflict of interest.

References

1. Klimova, M.; Stepanov, N.; Shaysultanov, D.; Chernichenko, R.; Yurchenko, N.; Sanin, V.; Zherebtsov, S. Microstructure and mechanical properties evolution of the Al, C-containing CoCrFeNiMn-type high-entropy alloy during cold rolling. *Materials* **2018**, *11*, 53. [CrossRef] [PubMed]
2. Xiong, T.; Zheng, S.; Pang, J.; Ma, X. High-strength and high-ductility $AlCoCrFeNi_{2.1}$ eutectic high-entropy alloy achieved via precipitation strengthening in a heterogeneous structure. *Scr. Mater.* **2020**, *186*, 336–340. [CrossRef]

3. Du, X.; Huo, X.; Chang, H.; Li, W.; Duan, G.; Huang, J.; Wu, B.; Zou, N.; Zhang, L. Superior strength-ductility combination of a Co-rich CoCrNiAlTi high-entropy alloy at room and cryogenic temperatures. *Mater. Res. Express* **2020**, *7*, 034001. [CrossRef]
4. Zhang, H.; Zhao, Y.; Huang, S.; Zhu, S.; Wang, F.; Li, D. Manufacturing and analysis of high-performance refractory high-entropy alloy via selective laser melting (SLM). *Materials* **2019**, *12*, 720. [CrossRef]
5. Ao, F.; Cao, Y.; Liu, Y.; Xu, S. Microstructure and mechanical properties of novel lightweight TaNbVTi-based refractory HEAs. *Materials* **2022**, *15*, 355.
6. Li, Y.; Liang, H.; Nie, Q.; Qi, Z.; Deng, D.; Jiang, H.; Cao, Z. Microstructures and wear resistance of $CoCrFeNi_2V_{0.5}Ti_x$ high-entropy alloy coatings prepared by laser cladding. *Crystals* **2020**, *10*, 352. [CrossRef]
7. Wu, M.; Chen, K.; Xu, Z.; Li, D. Effect of Ti addition on the sliding wear behavior of AlCrFeCoNi high-entropy alloy. *Wear* **2020**, *462*, 203493. [CrossRef]
8. Fu, A.; Liu, B.; Lu, W.; Liu, B.; Li, J.; Fang, Q.; Li, Z.; Liu, Y. A novel supersaturated medium entropy alloy with superior tensile properties and corrosion resistance. *Scr. Mater.* **2020**, *186*, 381–386. [CrossRef]
9. Wu, P.; Gan, K.; Yan, D.; Fu, Z.; Li, Z. A non-equiatomic FeNiCoCr high-entropy alloy with excellent anti-corrosion performance and strength-ductility synergy. *Corros. Sci.* **2021**, *183*, 109341. [CrossRef]
10. Liu, C.; Peng, W.; Jiang, C.S.; Gou, H.; Tao, J.; Deng, X.; Chen, Z. Composition and phase structure dependence of mechanical and magnetic properties for $AlCoCuFeNi_x$ high entropy alloys. *J. Mater. Sci. Technol.* **2019**, *35*, 1175–1183. [CrossRef]
11. Zhang, Y.; Qi, H.; Qu, Y.; Li, C.Z.; Lv, Q.; Li, Z.; Li, R.; Tan, B.; Tian, C.; Nie, S. The effect of TiC addition on the microstructure and mechanical properties of $Al_{0.6}CrFe_2Ni_2$ high entropy alloys. *SN Appl. Sci.* **2020**, *2*, 493. [CrossRef]
12. Tong, Z.; Ren, X.; Jiao, J.; Zhou, W.; Ren, Y.; Ye, Y.; Larson, E.A.; Gu, J. Laser additive manufacturing of FeCrCoMnNi high-entropy alloy: Effect of heat treatment on microstructure, residual stress and mechanical property. *J. Alloys Compd.* **2019**, *785*, 1144–1159. [CrossRef]
13. Xie, J.; Zhang, S.; Sun, Y.; Hao, Y.; An, B.; Li, Q.; Wang, C. Microstructure and mechanical properties of high entropy CrMnFeCoNi alloy processed by electopulsing-assisted ultrasonic surface rolling. *Mater. Sci. Eng. A* **2020**, *795*, 140004. [CrossRef]
14. Masemola, K.; Popoola, P.; Malatji, N. The effect of annealing temperature on the microstructure, mechanical and electrochemical properties of arc-melted AlCrFeMnNi equi-atomic high entropy alloy. *J. Mater. Res. Technol.* **2020**, *9*, 5241–5251. [CrossRef]
15. Shen, Q.; Kong, X.; Chen, X. Significant transitions of microstructure and mechanical properties in additively manufactured Al–Co–Cr–Fe–Ni high-entropy alloy under heat treatment. *Mater. Sci. Eng. A* **2021**, *815*, 141257. [CrossRef]
16. Mehranpour, M.; Shahmir, H.; Nili-Ahmadabadi, M. CoCrFeNiMn high entropy alloy microstructure and mechanical properties after severe cold shape rolling and annealing. *Mater. Sci. Eng. A* **2020**, *793*, 139884. [CrossRef]
17. Malatji, N.; Lengopeng, T.; Pityana, S.; Popoola, A.P.I. Effect of heat treatment on the microstructure, microhardness, and wear characteristics of AlCrFeCuNi high-entropy alloy. *Int. J. Adv. Manuf. Technol.* **2020**, *111*, 1–9. [CrossRef]
18. Munitz, A.; Salhov, S.; Guttmann, G.; Derimow, N.; Nahmany, M. Heat treatment influence on the microstructure and mechanical properties of $AlCrFeNiTi_{0.5}$ high entropy alloys. *Mater. Sci. Eng. A* **2019**, *742*, 1–14. [CrossRef]
19. Li, D.; He, W.; Zhang, X.; Xiao, M.; Li, S.; Zhao, K.; Yang, M. Effects of traditional heat treatment and a novel deep cryogenic treatment on microstructure and mechanical properties of low-carbon high-alloy martensitic bearing steel. *J. Iron Steel Res. Int.* **2021**, *28*, 370–382. [CrossRef]
20. Wannaprawat, N.; Tuchinda, K. Study of deep cryogenic treatment process effect on microstructure and properties of CuBeZr alloy. *Key Eng. Mater.* **2020**, *841*, 335–339. [CrossRef]
21. Cardoso, P.H.S.; Israel, C.L.; da Silva, M.B.; Klein, G.A.; Soccol, L. Effects of deep cryogenic treatment on microstructure, impact toughness and wear resistance of an AISI D6 tool steel. *Wear* **2020**, *456*, 203382. [CrossRef]
22. Li, C.; Qu, Y.; Zhang, Y.; Lv, Q.; Qi, H. Effect of deep cryogenic treatment on the microstructure and mechanical properties of $AlCrFe_2Ni_2$ high-entropy alloy. *Mater. Res. Express* **2020**, *7*, 036504. [CrossRef]
23. Zhang, W.; Bai, P.; Yang, J.; Xu, H.; Dang, J.; Du, Z. Tensile behavior of 3104 aluminum alloy processed by homogenization and cryogenic treatment. *Trans. Nonferrous Met. Soc. China* **2014**, *24*, 2453–2458. [CrossRef]
24. Bhale, P.; Shastri, H.; Mondal, A.K.; Masanta, M.; Kumar, S. Effect of deep cryogenic treatment on microstructure and properties of AE42 Mg alloy. *J. Mater. Eng. Perform.* **2016**, *25*, 3590–3598. [CrossRef]
25. Li, L.; Chen, H.; Fang, Q.; Li, J.; Liu, F.; Liu, Y.; Liaw, P.K. Effects of temperature and strain rate on plastic deformation mechanisms of nanocrystalline high-entropy alloys. *Intermetallics* **2020**, *120*, 106741. [CrossRef]
26. Singh, K.S.; Parashar, A. Effect of lattice distortion and nanovoids on the shock compression behavior of (Co-Cr-Cu-Fe-Ni) high entropy alloy. *Comput. Mater. Sci.* **2022**, *209*, 111402. [CrossRef]
27. Liu, J.; Chen, C.; Feng, Q.; Fang, X.; Wang, H.; Liu, F.; Lu, J.; Raabe, D. Dislocation activities at the martensite phase transformation interface in metastable austenitic stainless steel: An in-situ TEM study. *Mater. Sci. Eng. A* **2017**, *703*, 236–243. [CrossRef]

Disclaimer/Publisher's Note: The statements, opinions and data contained in all publications are solely those of the individual author(s) and contributor(s) and not of MDPI and/or the editor(s). MDPI and/or the editor(s) disclaim responsibility for any injury to people or property resulting from any ideas, methods, instructions or products referred to in the content.